J. Fluid Mech. (2026), *vol.* 1042, R3, doi:10.1017/jfm.2026.11981

JFM RAPIDS

Thermal convection in one, two, three and four dimensions

Ambrish Pandey[1,2], **Harshit Tiwari**[3] **and Katepalli R. Sreenivasan**[2,4]

[1]Department of Physics, Indian Institute of Technology Roorkee, Roorkee, Uttarakhand 247667, India

[2]Center for Astrophysics and Space Science, New York University Abu Dhabi, Abu Dhabi 129188, United Arab Emirates

[3]Department of Physics, Indian Institute of Technology Kanpur, Kanpur 208016, India

[4]Tandon School of Engineering, Department of Physics and Courant Institute of Mathematical Sciences, New York University, New York, NY 11201, USA

Corresponding authors: Katepalli R. Sreenivasan, katepalli.sreenivasan@nyu.edu; Ambrish Pandey, ambrishiitk@gmail.com

(Received 23 April 2026 UTC; revised 21 June 2026 UTC; accepted 28 July 2026 UTC)

We study by means of direct numerical simulations the influence of the dimensionality of convection on flow properties. We call attention to a few general principles from considering in totality the results from one dimension, two dimensions, three dimensions and four dimensions. In particular, we explore two practical aspects: (i) the transient time, or the amount of time it takes for the flow to reach the steady state; and (ii) possible implications for the so-called ultimate state.

Key words: turbulent convection, Bénard convection, turbulence simulation

1. Introduction

An increasing fraction of basic research on turbulent thermal convection is being drawn in recent years from direct numerical simulations (DNS). With this development, it has also become clearer that more attention needs to be paid to numerical convergence, resolution, transient time to steady state, etc. In this paper we attempt to understand transient times needed to achieve the steady state of convection in one dimension, two dimensions, three dimensions and four dimensions, and infer the advantages (or lack thereof) of studying convection in these different dimensions.

Pandey & Sreenivasan (2025) – PS henceforth – obtained transient times from the DNS of two-dimensional (2-D) Rayleigh–Bénard convection (RBC) in a box of aspect ratio

$\varGamma = 1$, and Prandtl numbers $Pr = 0.1$ and 1 and for Rayleigh numbers Ra between 10^6 and 10^{12}. (We define Ra, Pr and $\varGamma$ in § 2.) A main conclusion was that long transients with large-scale fluctuating heat transport accompany 2-D convection, which made observations of the ultimate state (Kraichnan 1962) quite uncertain. By the ultimate state, we refer to the asymptotic high-Ra regime where the Nusselt number scaling surpasses the classical $1/3$ exponent and approaches a power of $1/2$ (with possible logarithmic corrections).

As another variant of the practically important problem of 3-D convection, one may consider the case of four dimensions, for which the flow occurs in four spatial dimensions and time. There is no instance in the universe for which this configuration applies, yet there are good reasons to consider it. For instance, the Ising universality class has its upper critical dimension equal to 4. That is, for dimension $D \geqslant 4$ the renormalisation fixed point controlling the transition is Gaussian, so the leading critical exponents assume mean-field values, possibly with logarithmic corrections. It has been a long-held speculation that turbulence in four dimensions may also have normal scaling with no anomalies. For instance, will the 4-D convection adopt to the ultimate state at a manageably smaller Rayleigh number than in three dimensions?

To obtain a more complete perspective, we also consider heat transport in the 1-D setting. A moment's thought shows that, when the bottom of a 1-D convection system is heated and its top cooled, heat can be conveyed up only by conduction; there can never be any convection at any Ra or Pr. (One may interpret this result to mean that the transient state to convection is infinitely long.) In compressible cases, pressure perturbations can travel up and down but, again, there can be no convection. The oscillatory character of pressure has a dependence on Pr but the basic result is the same. We present the results only briefly in the body of the text and relegate details to the Supplementary Material (SM).

This paper is thus a study of the influence of dimensionality on thermal convection. Section 2 gives a brief discussion of the simulation parameters, while § 3 discusses the main results. It concludes with a few summary remarks and outlook in § 4. To be concise, we consistently refer to RBC in horizontally periodic boxes as RBC-P. The numerical code DHARA used to compute RBC-P is described and validated in the SM.

2. Simulation details

We perform DNS in 2-D, 3-D and 4-D settings assuming the Oberbeck–Boussinesq model

$$\nabla \cdot \boldsymbol{u} = 0, \tag{2.1}$$

$$\frac{\partial \boldsymbol{u}}{\partial t} + \boldsymbol{u} \cdot \nabla \boldsymbol{u} = -\frac{\nabla p}{\rho_0} + \alpha g (T - T_0)\hat{z} + \nu \nabla^2 \boldsymbol{u}, \tag{2.2}$$

$$\frac{\partial T}{\partial t} + \boldsymbol{u} \cdot \nabla T = \kappa \nabla^2 T, \tag{2.3}$$

where $\boldsymbol{u}(\boldsymbol{r})$, $p(\boldsymbol{r})$ and $T(\boldsymbol{r})$ are, respectively, velocity, pressure and temperature. The space dimensionality of the system is to be treated as appropriate. The acceleration due to gravity is $-g\hat{z}$; ρ_0 is the reference density, T_0 is the reference temperature and α, ν, κ are the isobaric thermal expansion coefficient, kinematic viscosity and thermal diffusivity, respectively. The dynamics of RBC is governed by $Ra = \alpha g \Delta T H^3/(\nu\kappa)$ and $Pr = \nu/\kappa$, where ΔT is the applied temperature difference between the bottom and top surfaces of the fluid layer of depth H. The flow velocities are measured in units of the free-fall velocity $u_f = \sqrt{\alpha g \Delta T H}$ and time scale in units of free-fall time $t_f = H/u_f$.

Pr	Ra	$N_e N^2$	Nu	Re	t_{sim} (t_f)
0.021	10^7	1150^2	10.97 ± 4.6	$22\,570 \pm 4986$	394
0.021	2×10^7	900^2	13.04 ± 5.2	$33\,921 \pm 7101$	557
0.021	3×10^7	1150^2	14.42 ± 5.7	$43\,040 \pm 8712$	496
0.021	5×10^7	2070^2	16.58 ± 7.0	$59\,928 \pm 11\,542$	136
0.021	10^8	2530^2	19.68 ± 10	$97\,012 \pm 17\,184$	220
0.021	4×10^8	3122^2	28.32 ± 20	$275\,539 \pm 19\,188$	106
0.021	10^9	4014^2	37.43 ± 28	$443\,526 \pm 53\,505$	159
0.05	10^7	700^2	12.41 ± 5.1	$11\,624 \pm 2588$	1177
0.05	2×10^7	700^2	14.52 ± 6.8	$16\,135 \pm 3401$	1370
0.05	3×10^7	900^2	16.06 ± 7.6	$20\,167 \pm 4497$	1008
0.05	10^8	1150^2	21.64 ± 10	$41\,298 \pm 7966$	763
0.05	3×10^8	1610^2	29.27 ± 16	$82\,321 \pm 20\,101$	632
0.05	5×10^8	1610^2	33.50 ± 20	$122\,255 \pm 25\,627$	882
0.05	10^9	2478^2	41.51 ± 27	$185\,128 \pm 30\,221$	250

Table 1. Important DNS parameters of RBC in a 2-D box of $\Gamma = 1$: $N_e N^2$ is the total number of mesh cells; t_{sim} is the total duration of simulation in the nominally steady state; Nu and Re are, respectively, the global heat and momentum transports in this state; the error bars are the corresponding standard deviations.

2.1. *Direct numerical simulations of 2-D convection*

In 2-D convection, the flow is constrained to a vertical plane, with $\boldsymbol{u}(\boldsymbol{r}) = (u_x, u_z)$ with $\boldsymbol{r} = (x, z)$. We first study the case of a no-slip condition at all walls, the horizontal walls being isothermal and the vertical walls adiabatic. In PS, we have already explored the characteristics of transients for $Pr = 0.1$ and $Pr = 1$ and for $10^6 \leqslant Ra \leqslant 10^{12}$. Here, we include Pr of 0.05 and 0.021. Direct numerical simulations of 2-D RBC, governed by (2.1)–(2.3), are conducted using a spectral element solver NEK5000 (Fischer 1997). The square domain is decomposed into N_e elements, further discretised using N*th*-order Legendre polynomials. Details of DNS for $Pr = 0.1$ and $Pr = 1$ can be found in PS, and those for $Pr = 0.021$ in Pandey (2021). Additional details for $Pr = 0.021$ and $Pr = 0.05$ are provided in table 1.

To make direct comparisons with $D = 3$ and $D = 4$, we have performed simulations of 2-D convection also for $\Gamma = 1$, with periodic sidewalls (RBC-P). These simulations are conducted using the incompressible module of the finite-difference code DHARA (see SM). The gross flow response quantities are summarised in table 2.

2.2. *Direct numerical simulations of 3-D convection*

We consider the following configurations with no-slip and isothermal top and bottom walls: (*a*) closed cube with no-slip condition at all the walls; (*b*) closed rectangular cuboid of length $2.4H$ and width $0.8H$ (Pandey *et al.* 2026), especially to understand the effects of geometry; and (*c*) cube with periodic sidewalls (RBC-P). The sidewalls in (*a*) and (*b*) are adiabatic. The DNS of RBC are performed for $Pr = 0.1$, 1, 10 for Ra between 10^6 and 10^{10}. The higher-Ra simulations are carried out on coarser meshes than demanded for a faithful replication of the entire flow structure, but the conclusions on transients do not depend on the resolution, up to a point. In the SM, we examine the consequences of using coarser resolutions on transients; see also PS. The RBC-P cases for $Pr = 1$ are conducted using the incompressible module of the finite-difference code DHARA, as summarised in table 2.

		$D=2$			$D=3$			$D=4$		
Ra	N	Nu	Re	t_{sim}	Nu	Re	t_{sim}	Nu	Re	t_{sim}
2×10^5	64	4.8 ± 3.8	94 ± 30	200	7.4 ± 0.1	98 ± 1	200	7.9 ± 0.1	100 ± 1	200
5×10^5	64	6.2 ± 3.2	173 ± 19	500	8.9 ± 0.4	145 ± 6	200	9.2 ± 0.3	147 ± 6	200
10^6	64	6.9 ± 5.3	254 ± 34	500	10.4 ± 0.8	202 ± 6	200	11.1 ± 0.3	205 ± 6	200
2×10^6	64	8.5 ± 5.2	385 ± 33	500	11.3 ± 0.7	277 ± 7	200	13.1 ± 0.3	278 ± 7	200
5×10^6	128	10.3 ± 5.4	656 ± 29	500	14.3 ± 0.6	412 ± 20	200	16.1 ± 0.5	411 ± 20	200
10^7	128	11.8 ± 4.2	955 ± 19	500	17.5 ± 0.8	592 ± 13	200	19.9 ± 0.4	577 ± 13	200
2×10^7	128	13.1 ± 4.5	1457 ± 22	500	20.6 ± 0.8	780 ± 18	200	23.7 ± 0.6	793 ± 18	200
5×10^7	256	13.3 ± 5.5	2595 ± 21	1000	26.5 ± 0.8	1229 ± 28	200	31.1 ± 0.7	1230 ± 28	100
10^8	256	13.6 ± 5.5	3865 ± 20	1000	32.6 ± 0.8	1624 ± 30	200	37.6 ± 0.8	1680 ± 30	100
2×10^8	256	15.5 ± 6.9	5696 ± 22	1000	39.1 ± 0.8	2333 ± 42	200	45.7 ± 0.9	2390 ± 42	100
5×10^8	512	20.4 ± 13.4	9933 ± 30	1000	—	—	—	—	—	—
10^9	512	24.6 ± 18.1	$14\,624\pm38$	1000	—	—	—	—	—	—

Table 2. Response quantities for RBC-P in $D=2$, 3 and 4, $Pr=1$. N is the number of grid points for each spatial dimension (accounting for a total of N^D points) used by the finite-difference solver DHARA. Here, Nu and Re values are time averaged, with $\pm$ one standard deviation; t_{sim} is the integration time in units of t_f.

2.3. *Direct numerical simulations of 4-D convection*

Four-dimensional convection is performed in a periodic hypercube of size $L_w=L_x=L_y=H$ for $Pr=1$ and Rayleigh numbers between $Ra=10^5$ and 2×10^8. To ensure a direct comparison, 2-D and 3-D simulations are conducted using a consistent numerical framework, as summarised in table 2. These cases utilise the incompressible module of the finite-difference solver DHARA, which employs a second-order spatial discretisation on a staggered marker-and-cell grid and a third-order Runge–Kutta scheme for time integration.

The computational complexity of 4-D simulations increases strongly with Ra. Even for $Ra=2\times10^8$, which was resolved on a 256^4 grid, it represented approximately 4.3 billion degrees of freedom per variable. This specific run was executed on 128 NVIDIA A100 GPUs across 32 compute nodes on the Polaris supercomputer at the Argonne Leadership Computing Facility (ALCF). This simulation required approximately 18 wall-clock hours to reach an integration time of $t_{sim}=100$.

3. Results

3.1. *Basic response quantities*

The instantaneous state of convection is given by the domain-averaged kinetic energy

$$E=\langle|\boldsymbol{u}|^2/2\rangle_V/u_f^2. \tag{3.1}$$

Here, we have $E=0$ in the purely diffusive state of no motion, and $E>0$ represents a perturbed state. Temporal evolution of the flow can be described by the evolution of E. Once convection is established and the system is in a statistically steady state, the flow strength is measured by the Reynolds number Re, which is commonly defined in DNS studies using the root-mean-square (r.m.s.) velocity

$$Re=u_{rms}H/\nu, \quad \text{where} \quad u_{rms}=\sqrt{\langle|\boldsymbol{u}|^2\rangle_{V,t}}. \tag{3.2}$$

Here, $\langle\cdot\rangle_{V,t}$ is the average over the entire domain, and also time in the statistically steady state. The mean kinetic energy in this state is defined as $E_{av}=0.5u_{rms}^2/u_f^2$.

The heat transport through the convective layer is quantified using the Nusselt number

$$Nu = 1 + \frac{H}{\kappa \Delta T} \langle u_z T \rangle_{V,t}. \tag{3.3}$$

The globally averaged kinetic energy and thermal dissipation rates can also be used to define Nusselt numbers; their closeness to *Nu* from (3.3) is thought to ensure the spatial and temporal convergence (see Stevens *et al.* 2010 and PS). We have verified that the Nusselt numbers computed using different methods agree within a few per cent.

3.2. *One-dimensional flow*

Conduction is the only means of transport between top and bottom walls in the incompressible case. While the continuity equation, $\partial(\rho u_z)/\partial z = -\partial \rho / \partial t$ (where ρ is the density of the fluid), allows for local density variations in the compressible case, the strictly 1-D geometry and impenetrable boundaries at the top and bottom prevent vertical mass flux or bodily overturning – hence no convection. A linear instability analysis and the DNS (both detailed in the SM) confirm this constraint. The determinant of the linearised system is strictly non-zero for all real wavenumbers, mathematically precluding the stationary bifurcation required for classical convection. The system does support oscillatory acoustic modes as *Ra* increases, but these purely longitudinal compressions do not lead to heat transport with a unidirectional motion. (Professor J. Wettlaufer has suggested a possible connection of the present 1-D considerations to highly confined quasi-1-D superfluid systems: there will be no convection in such systems either, but its detailed discussion here takes us too far from the theme of the paper.)

3.3. *Two-dimensional convection*

We showed in PS, for $10^7 \leqslant Ra \leqslant 10^{12}$, that the scaling of the transient time varies in the range $Ra^{0.6}$ to $Ra^{0.7}$, consistent with Lindborg's theory (Lindborg 2025), but the coefficient of proportionality depended on *Pr*. We note that Lindborg's theoretical lower bound corresponds to the global diffusion time H^2/ν, and the transient times observed in our simulations actually exceed this time scale. Recall that the r.m.s. velocity of turbulent convective flows in a 2-D domain does not scale as the free-fall velocity; it is a function of *Ra* and *Pr*. In addition, PS found that u_{rms}/u_f scales as $Ra^{1/6} Pr^{-1/2}$ in the high-*Re* regime. This scaling suggests that, in 2-D RBC, it takes longer with increasing *Ra* or decreasing *Pr* to achieve the nominally steady state. This is demonstrated in figure 1, where temporal evolutions of E in a 2-D square box are shown for various *Ra*, and $Pr = 0.021$. Figure 1(*b*) shows that E in the initial phase grows exponentially when the convective motion is getting established. However, as seen better in figure 1(*a*), this initial exponential is followed by another slow exponential growth in the convection state. Only after this extended second growth state does E begin to attain a nominal mean that increases with *Ra*, with huge fluctuations around it.

For a simulation performed *ab initio* from the conduction state, E evolves in the slow exponential state of convection according to

$$[E_{av} - E(t)]/E_{av} = c \exp(-kt), \tag{3.4}$$

where c is the scaling factor and k is the growth rate (see PS). The transient time t_{trns} is defined as the time that is required for the flow to reach a state, where E is a certain fraction of E_{av}. Taking, for example, $E = 0.96 E_{av}$ in (3.4), the transient time is computed as

$$t_{trns} = \frac{1}{k} \log \frac{c}{0.04}. \tag{3.5}$$

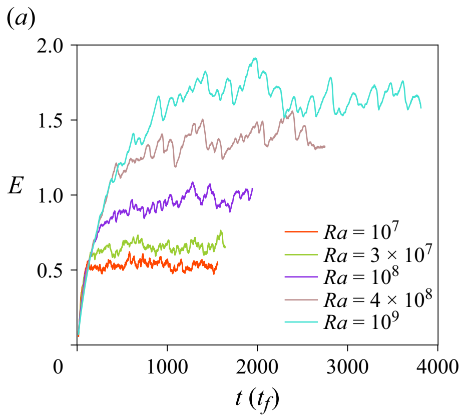

Figure 1. (*a*) Evolution of E for different Rayleigh numbers at $Pr = 0.021$ in a closed 2-D square box. Time required to achieve a nominally steady state increases with Ra. (*b*) Energy growth is exponential during the initial phase when the perturbations grow and convective motion is being established. (There are of the order of 100 data points in the initial exponential part.)

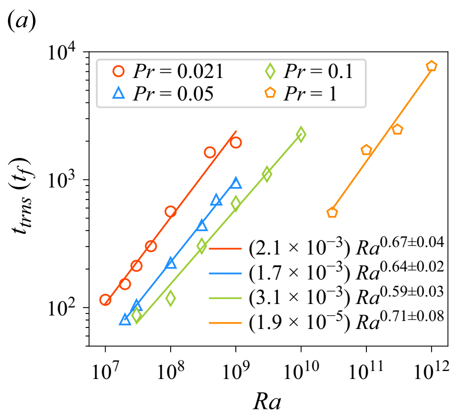

Figure 2. Transient time t_{trns} for RBC in a 2-D square box as a function of (*a*) Rayleigh number and (*b*) Reynolds number. Solid lines represent best fits. Scaling exponents in (*a*) depend on Pr. Solid black line in (*b*) is the best fit using data for all Pr. Data for $Pr = 1$ and $Pr = 0.1$ are taken from PS.

Transient times t_{trns} estimated using (3.5), plotted against Ra in figure 2(*a*), show an increase with Ra. The best fit exponents vary between 0.59 and 0.71 depending on Pr. Consistent with the trend found in PS, they become longer with decreasing Pr for a fixed thermal forcing. Figure 2(*b*) shows t_{trns} as a function of the flow Reynolds number; data for different Prandtl numbers nearly collapse and the best fits are approximately linear in Re. The best fit for data at all Pr yields $t_{trns} = 0.0044Re^{1.02}$.

It should be stressed that these data are applicable for *ab initio* calculations (i.e. convection begun from slightly perturbed conduction states). As the steady state kinetic energy is higher for higher Ra, there will be a transient period also when the simulation is begun from the lower Ra. However, those transient times will be shorter than for the *ab initio* simulations. The observed linear dependence of the transient time on Re imposes

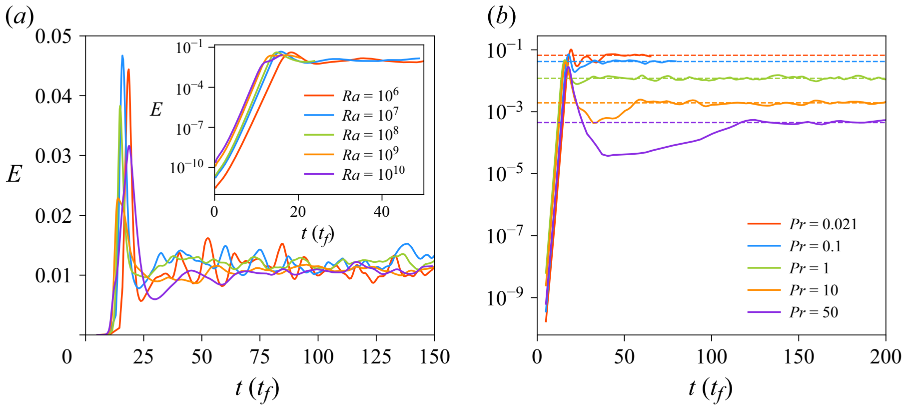

Figure 3. Temporal evolution of E for RBC in a closed cubic domain (*a*) for various Ra at $Pr = 1$, and (*b*) for different flows at $Ra = 10^7$. Inset in (*a*) reveals that the growth in the initial phase during the setting up of the convective motion is exponential in nature. Dashed horizontal lines in (*b*) indicate E_{av}.

severe restrictions on the exploration of 2-D convection at high Re – as could, in fact, be inferred already from Lindborg (2025).

3.4. *Three-dimensional convection*

This is the practically relevant case. In figure 3(*a*), the evolutions of E for RBC in a closed cubic domain for $Pr = 1$ and $10^6 \leqslant Ra \leqslant 10^{10}$ are shown, where the simulations begin from the diffusive state. We observe that E grows rapidly in the beginning and starts to fluctuate, achieving a plausible E_{av} beyond 50 to 70 t_f. The inset of figure 3(*a*), where E is shown on a logarithmic scale, reveals that the initial growth is exponential as in two dimensions, when the convective motion is getting established. Qualitatively similar evolutions of E occur for flows at $Pr = 0.1$ and $Pr = 10$. The same is true also for flows in a rectangular cuboid of dimensions $L_x = 2.4H$ and $L_y = 0.8H$ (Pandey *et al.* 2026) – see the SM. Note that, unlike in two dimensions, the variation of E_{av} with Ra is weaker for $Pr \approx 1$, although E_{av} decreases slightly with Ra for low-Pr fluids, while it increases slightly for high-Pr fluids. This is also inferred from the scaling of the Reynolds number in 3-D convection: $Re \sim Ra^{1/2}$ for $Pr \sim 1$ (Chillà & Schumacher 2012; Pandey *et al.* 2026), $Re \sim Ra^{0.44}$ for $Pr \lesssim 0.03$ (Pandey & Verma 2016; Scheel & Schumacher 2017) and $Re \sim Ra^{0.6}$ for $Pr \gg 1$ (Silano *et al.* 2010; Horn *et al.* 2013; Pandey *et al.* 2014).

Evolution of E for different Pr and $Ra = 10^7$ in the same cubic domain is shown in figure 3(*b*). Note that E_{av}, and thus Re, decreases with increasing Pr (Pandey & Sreenivasan 2021). The logarithmic scale for E in figure 3(*b*) highlights the exponential growth in the beginning, and also a strong dependence of E_{av} on Pr. The steady state takes slightly longer with increasing Pr; thus, it seems that the transient time in three dimensions increases, albeit weakly, with decreasing Re. However, as a whole, the trends with respect to Ra or Re are not strong as in two dimensions (as one might indeed have expected).

3.5. *Four-dimensional convection*

3.5.1. *Motivation*

Here, we consider convection in four spatial dimensions and time. Since 4-D convection never appears in the universe, a few sentences are useful to justify the effort. We recall that Wilson & Fisher (1972) considered systems with spatial dimension of $4 - \epsilon$, where $\epsilon \ll 1$.

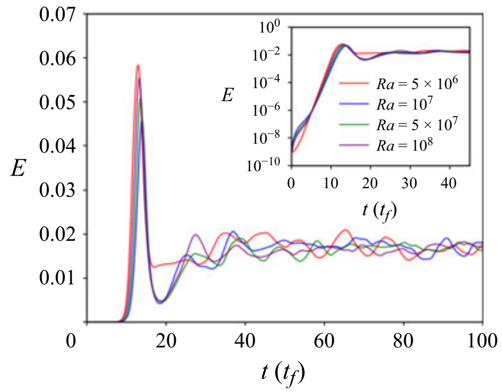

Figure 4. Temporal evolution of the domain-averaged kinetic energy E in a 4-D horizontally periodic domain for $Pr = 1$ at various Rayleigh numbers. Similar to the 3-D case, the inset reveals an initial phase of exponential growth as the convective motion is established, followed by a statistically steady state where E fluctuates around its mean value E_{av}.

Their insight was that four dimensions is the upper critical dimension for equilibrium phase transitions, and that Landau's mean-field theory becomes exact for four dimensions and beyond, with deviations from it arising in fewer dimensions. Indeed, they showed that one can treat the deviation perturbatively in ϵ. Nelkin (1974, 1975) proposed that four spatial dimensions might play an analogous role in turbulence theory, and argued that intermittency arises from fluctuations of the local energy dissipation and cascade transfer rates, which would weaken with increasing dimension. If this conjecture is true, $D = 4$ would behave like a mean-field limit for turbulence. This has never been proven, despite some suggestion (Gotoh *et al.* 2007; Yamamoto *et al.* 2012) that intermittency weakens with increasing dimensions. The last two papers studied homogeneous and isotropic turbulence.

One of the problems in drawing firm conclusions from these studies is that the DNS in higher dimensions becomes more expensive and so the Reynolds numbers of the DNS are smaller. Although, because of this, it was clear from the outset that the Rayleigh numbers achievable would be quite modest in four dimensions, we regarded that some instructive lesson could arise while making comparisons with three dimensions.

3.5.2. *Results*

The results of 4-D simulations are summarised in table 2 for $Pr = 1$. Due to the high computational cost associated with the N^4 grid scaling, these runs currently span Rayleigh numbers from 10^5 to 2×10^8, but are adequate for drawing a preliminary conclusion.

As shown in figure 4, the temporal evolution of the kinetic energy E in four dimensions is similar to that in three dimensions. After a slightly perturbed conduction state, there is an initial exponential growth phase in which the convective motion is established. The system later enters a statistically steady state characterised by fluctuations around the mean value E_{av}. The transient time for reaching this steady state in four dimensions is approximately 40 to 50 t_f, which is somewhat smaller than in three dimensions but comparable overall. The transient times show an increasingly weaker trend with Re as the dimensionality increases beyond 2; the 3-D and 4-D cases are similar in this regard.

However, the Nusselt and Reynolds numbers, presented in figure 5, depend on the dimensionality of convection. Figure 5(a) shows that the Nusselt number at a given Ra

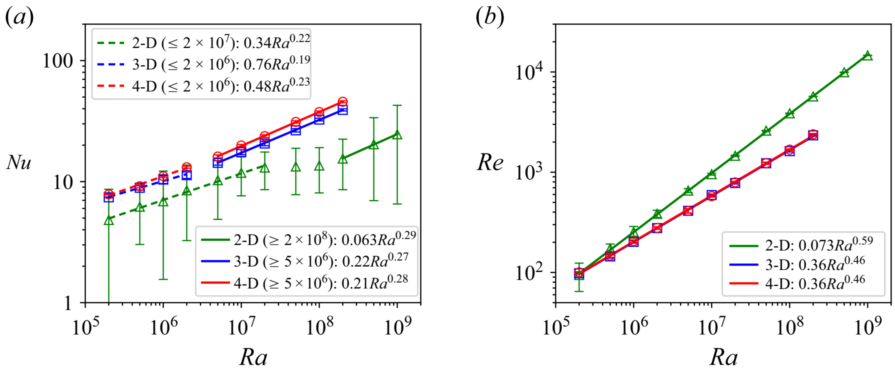

Figure 5. Scaling of global response quantities with Ra for RBC-P at $Pr = 1$ in $D = 2$, 3 and 4. (*a*) Nusselt number (Nu) versus Ra. Dashed and solid lines represent power-law fits for low- and moderate-Ra regimes, respectively. (*b*) Reynolds number (Re) versus Ra with global power-law fits. Error bars denote the standard deviation of temporal fluctuations.

increases with D, although the difference is less conspicuous between three and four dimensions than it is between two and three dimensions. For example, in the range $Ra \geqslant 5 \times 10^6$, the scalings for three dimensions ($Nu = 0.22 Ra^{0.27}$) and four dimensions ($Nu = 0.21 Ra^{0.28}$) share closely similar powers and prefactors. By comparison, the scaling in two dimensions follows $Nu = 0.063 Ra^{0.29}$, although characterised by massive temporal fluctuations. The overall enhancement of Nu in higher dimensions stems from the increased spatial degrees of freedom, which allow thermal plumes to advect heat with significantly fewer disruptive interactions. For $Ra = 2 \times 10^8$, Nu in three dimensions is roughly 2.4 times that in two dimensions, while that in four dimensions it is only 15 % higher than that in three dimensions. Two-dimensional data show a conspicuous break for a decade around $Ra = 10^8$, which is due to the appearance of a strong zonal flow (Goluskin *et al.* 2014) for this range of Ra. The flow structures and their evolutions suggest that 2-D convective flows in a horizontally periodic box of $\Gamma = 1$ comprise a strong zonal component for all higher-Ra cases in the present work. Consequently, the heat transport is lower than that in a closed square box, as reported by Pandey & Sreenivasan (2025).

Figure 5(*b*) further highlights a striking difference between two dimensions, on the one hand, and three and four dimensions, on the other: the Reynolds number is higher in two dimensions ($Re = 0.071 Ra^{0.59}$) compared with the lower (and nearly indistinguishable) scalings of three and four dimensions ($Re \approx 0.36 Ra^{0.46}$). Rather than indicating more intense small-scale turbulence, this elevated Re in two dimensions is a consequence of enstrophy conservation, which prohibits vortex stretching and forces an inverse cascade of kinetic energy. The resulting accumulation of energy in the largest available scales generates a domain-filling large-scale circulation that inflates the r.m.s. velocity. In three and four dimensions, the availability of vortex stretching enables a forward energy cascade to dissipative scales, severely weakening this domain-sized scale and yielding lower Reynolds numbers. Note that the scaling exponent in two dimensions in the horizontally periodic domain is smaller than 2/3, which was derived by Lindborg (2025) and confirmed numerically by Pandey & Sreenivasan (2025). However, we stress that the scaling $Re \sim Ra^{2/3}$ is realised only at high enough Rayleigh numbers. Pandey & Sreenivasan (2025) observed that the Re in the closed square domain exhibits a shallower scaling at lower Rayleigh numbers. In fact, their data for Ra between 10^7 and 10^9 for $Pr = 1$ are consistent with a $Re \sim Ra^{0.59}$ scaling, very similar to that found here.

These scaling behaviours also provide a context for commenting on convection at extreme thermal forcing. One might have expected that the additional spatial degree of freedom in four dimensions would trigger a transition to a new scaling regime at a comparatively lower Ra. However, our results show that the near-classical power law persists in four dimensions up to $Ra = 2 \times 10^8$. The robustness of these scaling exponents in three and four dimensions suggests that spatial dimensionality does not bypass the fundamental, classical mechanisms of heat transport. Consequently, what ultimately happens to the flow at exceptionally high Rayleigh numbers may remain essentially the same, demanding similarly high levels of thermal forcing for all spatial dimensions.

4. Summary remarks and outlook

In this study, we have explored the influence of spatial dimensionality, ranging from 1 to 4, on the dynamics of thermal convection. We find that the transient time required to achieve a statistically steady convective state is fundamentally tied to the geometric constraints of the system. In the degenerate 1-D case, strict constraints prohibit convection physically and mathematically. In two dimensions, the transient times are exceptionally long and scale approximately linearly with the flow Reynolds number, posing a severe computational bottleneck for exploring very high-Ra regimes. As the dimensionality increases to three and four dimensions, the dependence of the transient duration on Re becomes markedly weaker. The temporal evolution of the kinetic energy in four dimensions closely mirrors that of three dimensions, confirming that the transition to a steady state becomes more efficient and less dependent on thermal forcing when sufficient spatial degrees of freedom are available.

Based on our findings on the transient time in systems of dimensions one to four, we construct the following empirical relation:

$$\text{Transient time}/t_f = \beta Re^{\eta}, \quad \text{where} \quad \eta = \frac{(D-3)(D-4)}{2(D-1)}. \tag{4.1}$$

The prefactor $\beta \approx 40$ for three and four dimensions, whereas $\beta \approx 4.4 \times 10^{-3}$ for two dimensions.

We may now state our conclusions as follows. First, given the long transient times in two dimensions, it appears that a decisive study of the ultimate state of convection in two dimensions requires an unduly long computational time – which, in fact, may never be possible at extremely high Reynolds numbers. Second, for 3-D convection, t_{trns} is of the order of 50 free-fall times. Third, if it is possible to treat 3-D convection as a perturbation of 4-D convection, there may be some merit to studying 4-D convection to determine various scaling problems, including the ultimate state. However, even if the 4-D case behaves like the mean-field model and the 3-D case can be conceived as a perturbation from four dimensions, we should expect that, at the level of accuracy with which we have been able to determine the transient times, we should not expect in this regard a huge differences between the 3-D and 4-D cases.

Supplementary material. Supplementary material is available at https://doi.org/10.1017/jfm.2026.11981.

Acknowledgements. We thank Shreshthi for providing data of figure 3(*b*) in the SM, and J. Wettlaufer for comments on a preliminary draft. The authors gratefully acknowledge Dalma and Jubail clusters at NYU Abu Dhabi for providing computational resources. We also thank ALCF for computing time on Polaris via the Director's Discretionary Program.

Funding. This material is based upon work supported by Tamkeen under the NYU Abu Dhabi Research Institute grant G1502. A.P. also acknowledges financial support from ANRF (formerly SERB), India under the grant SRG/2023/001746. H.T. thanks IIT Kanpur for the Fellowship for Academic and Research Excellence (FARE). NYU supports the research of K.R.S.

Declaration of interests. The authors report no conflict of interest.

Data availability statement. The data that support the findings of this study are available from the corresponding author upon reasonable request.

References

CHILLÀ, F. & SCHUMACHER, J. 2012 New perspectives in turbulent Rayleigh–Bénard convection. *Eur. Phys. J. E* **35**, 58.

FISCHER, P.F. 1997 An overlapping Schwarz method for spectral element solution of the incompressible Navier–Stokes equations. *J. Comput. Phys.* **133** (1), 84–101.

GOLUSKIN, D., JOHNSTON, H., FLIERL, G.R. & SPIEGEL, E.A. 2014 Convectively driven shear and decreased heat flux. *J. Fluid Mech.* **759**, 360–385.

GOTOH, T., WATANABE, Y., SHIGA, Y., NAKANO, T. & SUZUKI, E. 2007 Statistical properties of four-dimensional turbulence. *Phys. Rev. E* **75**, 016310.

HORN, S., SHISHKINA, O. & WAGNER, C. 2013 On non-Oberbeck–Boussinesq effects in three-dimensional Rayleigh–Bénard convection in glycerol. *J. Fluid Mech.* **724**, 175–202.

KRAICHNAN, R.H. 1962 Turbulent thermal convection at arbitrary Prandtl number. *Phys. Fluids* **5** (11), 1374–1389.

LINDBORG, E. 2025 Scaling in two-dimensional Rayleigh–Bénard convection. arXiv: 2506.13213.

NELKIN, M. 1974 Turbulence, critical fluctuations, and intermittency. *Phys. Rev. A* **9**, 388–395.

NELKIN, M. 1975 Scaling theory of hydrodynamic turbulence. *Phys. Rev. A* **11**, 1737–1743.

PANDEY, A. 2021 Thermal boundary layer structure in low-Prandtl-number turbulent convection. *J. Fluid Mech.* **910**, A13.

PANDEY, A., SCHUMACHER, J., PARSANI, M. & SREENIVASAN, K.R. 2026 Influence of plume activity on thermal convection in a rectangular cell. *J. Fluid Mech.* **1034**, A41.

PANDEY, A. & SREENIVASAN, K.R. 2021 Convective heat transport in slender cells is close to that in wider cells at high Rayleigh and Prandtl numbers. *Europhys. Lett.* **135** (2), 24001.

PANDEY, A. & SREENIVASAN, K.R. 2025 Transient and steady convection in two dimensions. *J. Fluid Mech.* **1015**, A42.

PANDEY, A. & VERMA, M.K. 2016 Scaling of large-scale quantities in Rayleigh–Bénard convection. *Phys. Fluids* **28** (9), 095105.

PANDEY, A., VERMA, M.K. & MISHRA, P.K. 2014 Scaling of heat flux and energy spectrum for very large Prandtl number convection. *Phys. Rev. E* **89**, 023006.

SCHEEL, J.D. & SCHUMACHER, J. 2017 Predicting transition ranges to fully turbulent viscous boundary layers in low Prandtl number convection flows. *Phys. Rev. Fluids* **2**, 123501.

SILANO, G., SREENIVASAN, K.R. & VERZICCO, R. 2010 Numerical simulations of Rayleigh–Bénard convection for Prandtl numbers between 10^{-1} and 10^4 and Rayleigh numbers between 10^5 and 10^9. *J. Fluid Mech.* **662**, 409–446.

STEVENS, R., VERZICCO, R. & LOHSE, D. 2010 Radial boundary layer structure and Nusselt number in Rayleigh–Bénard convection. *J. Fluid Mech.* **643**, 495–507.

WILSON, K.G. & FISHER, M.E. 1972 Critical exponents in 3.99 dimensions. *Phys. Rev. Lett.* **28**, 240–243.

YAMAMOTO, T., SHIMIZU, H., INOSHITA, T., NAKANO, T. & GOTOH, T. 2012 Local flow structure of turbulence in three, four, and five dimensions. *Phys. Rev. E* **86**, 046320.

Supplemental Material: Thermal convection in 1, 2, 3 and 4 dimensions

Ambrish Pandey,[1,2] Harshit Tiwari,[3] and Katepalli R. Sreenivasan[2,4]

[1] *Department of Physics, Indian Institute of Technology Roorkee, Roorkee 247667, Uttarakhand, India*
[2] *Center for Astrophysics and Space Science, New York University Abu Dhabi, Abu Dhabi 129188, United Arab Emirates*
[3] *Department of Physics, Indian Institute of Technology Kanpur, Kanpur 208016, India*
[4] *Tandon School of Engineering, Department of Physics and Courant Institute of Mathematical Sciences, New York University, New York, NY 11201, USA*

This Supplementary Material provides the linear stability analysis of a 1D system by investigating the case of a compressible fluid obeying the ideal gas law, and includes some relevant numerical results. It also provides some details of the incompressible code (named DHARA) for 2D, 3D and 4D convection. It also examines the dependence of the transient time on the numerical resolution as well as on the shape of the convection domain.

S1. ONE-DIMENSIONAL COMPRESSIBLE CONVECTION

A. Linear Instability Analysis

For a fluid contained between $z = 0$ and $z = H$, subjected to a constant gravitational acceleration g in the $-\hat{z}$ direction, the governing equations for mass, momentum, and energy conservation, along with the equation of state, are [1]:

$$\partial_t \rho + \partial_z(\rho u) = 0, \tag{S1}$$

$$\rho(\partial_t u + u\partial_z u) = -\partial_z p - \rho g + \frac{4}{3}\mu \partial_{zz} u, \tag{S2}$$

$$C_v \rho(\partial_t T + u\partial_z T) = -p\partial_z u + K\partial_{zz} T + \frac{8}{9}\mu(\partial_z u)^2, \tag{S3}$$

$$p = R_* \rho T, \tag{S4}$$

where we have used the standard notation. The parameters μ and K stand for the dynamic viscosity and thermal conductivity of the fluid, respectively; C_v denotes the specific heat at constant volume and R_* the gas constant. We non-dimensionalize these equations using the box height H and the bottom plate temperature (T_b) and density (ρ_b) as characteristic scales. The free-fall velocity $u_f = \sqrt{\epsilon_s g H}$. We thus have five non-dimensional control parameters:

$$\gamma = \frac{C_p}{C_v}, \quad \epsilon_s = \frac{H}{T_b}\left(\frac{\Delta T}{H} - \frac{g}{C_p}\right), \quad Di = \frac{gH}{C_p T_b}, \quad Ra = \frac{\epsilon_s g H^3}{\nu\kappa}, \quad Pr = \frac{\nu}{\kappa}. \tag{S5}$$

Here, Di is the *dissipation number* and ϵ_s is the *superadiabaticity*, and C_p is the specific heat at constant pressure. The dissipation number characterizes the fractional temperature drop across the domain purely due to the adiabatic expansion of a vertically displaced fluid parcel [2]. The superadiabaticity quantifies the dimensionless excess of the imposed temperature gradient over this adiabatic gradient. As extensively discussed in recent literature on fully compressible and strongly stratified Rayleigh-Bénard convection [2–5], the relative magnitudes of ϵ_s and Di dictate the flow's compressibility regime and govern the departure from the Boussinesq or anelastic approximations. According to the Schwarzschild criterion, the onset of convection requires a superadiabatic background, dictating that $\epsilon_s > 0$ for instability. In non-dimensional terms, the governing equations become:

$$\partial_t \rho + \partial_z(\rho u) = 0, \tag{S6}$$

$$\rho(\partial_t u + u\partial_z u) = -\partial_z p - \frac{1}{\epsilon_s}\rho + \frac{4}{3}\sqrt{\frac{Pr}{Ra}}\partial_{zz} u, \tag{S7}$$

$$\frac{1}{\gamma \epsilon_s Di}\rho(\partial_t T + u\partial_z T) = -p\partial_z u + \frac{1}{\epsilon_s Di\sqrt{PrRa}}\partial_{zz} T + \frac{8}{9}\sqrt{\frac{Pr}{Ra}}(\partial_z u)^2, \tag{S8}$$

$$p = \frac{1}{\epsilon_s Di(1+\alpha_a)}\rho T, \tag{S9}$$

where $\alpha_a = 1/(\gamma-1)$ is the adiabatic index.

We fix the temperatures at the boundaries ($T(0)=1$, $T(1)=1-Di-\epsilon_s$) and apply no-slip conditions ($u(0)=u(1)=0$). Expanding the variables into a conduction profiles and small perturbations, we write $T(z,t)=T_0(z)+T'(z,t)$ and $\rho(z,t)=\rho_0(z)+\rho'(z,t)$. The base states are $T_0(z)=1-(\epsilon_s+Di)z$ and $\rho_0(z)=T_0^m(z)$. The polytropic index is defined as

$$m = \frac{Di(1+\alpha_a)}{\epsilon_s+Di} - 1. \tag{S10}$$

Following classical compressible stability theory [6], the Schwarzschild criterion for the onset of convection can be expressed as $\alpha_a > m$. Expanding ρ and T in the non-dimensionalized equations and retaining only the linear terms, we obtain the following linearized equations:

$$\partial_t \rho' = [(\epsilon_s+Di)m - \partial_z]\, u, \tag{S11}$$

$$\partial_t u = -\frac{1}{\epsilon_s Di(1+\alpha_a)}\left[(\partial_z-(\epsilon_s+Di))\rho' + (\partial_z - m(\epsilon_s+Di))T'\right] - \frac{\rho'}{\epsilon_s} + \frac{4}{3}\sqrt{\frac{Pr}{Ra}}\partial_{zz}u, \tag{S12}$$

$$\partial_t T' = \gamma\epsilon_s Di((\epsilon_s+Di)-\partial_z)u + \frac{\gamma}{\sqrt{PrRa}}\partial_{zz}T'. \tag{S13}$$

For analytical calculation, we apply a standard normal mode analysis [7] and assume periodic perturbations of the form $\phi'(z,t)=\hat{\phi}(k,t)e^{ikz}$. Defining $\zeta=\epsilon_s+Di$ and $C_1=1/[\epsilon_s Di(1+\alpha_a)]$, the system is cast into matrix form $\partial_t\mathbf{v}=\mathbf{M}\mathbf{v}$, where $\mathbf{v}=[\hat{\rho}',\hat{u},\hat{T}']^{\mathrm{T}}$, as:

$$\mathbf{M} = \begin{bmatrix} 0 & \zeta m - ik & 0 \\ -C_1(ik-\zeta) - \frac{1}{\epsilon_s} & -\frac{4}{3}\sqrt{\frac{Pr}{Ra}}k^2 & -C_1(ik-m\zeta) \\ 0 & \gamma\epsilon_s Di(\zeta-ik) & -\frac{\gamma}{\sqrt{PrRa}}k^2 \end{bmatrix}. \tag{S14}$$

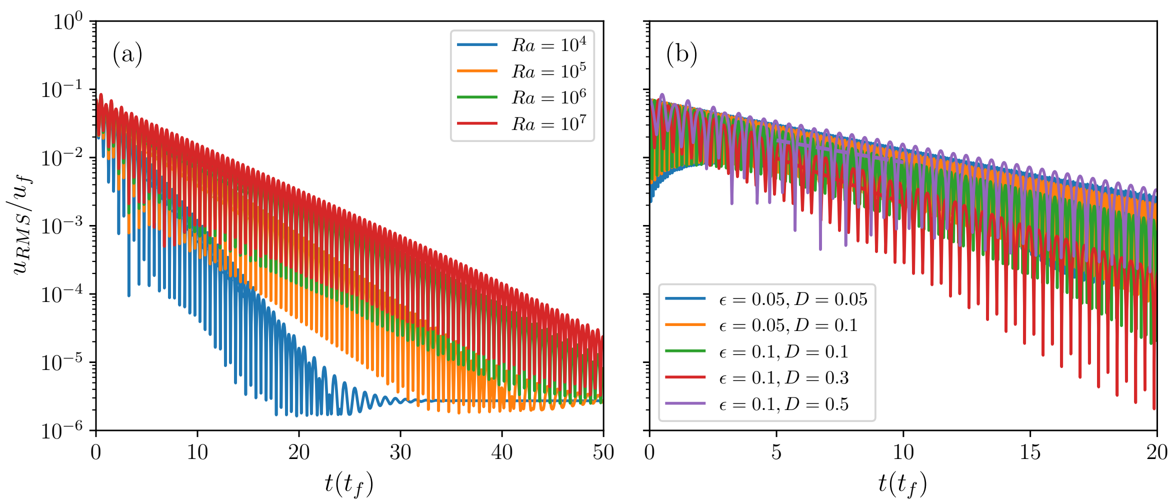

FIG. S1. Temporal evolution of the non-dimensionalized root-mean-square velocity u_{RMS}/u_f following a large initial perturbation ($\sim 0.1u_f$) in 1D compressible convection. (a) Oscillatory decay for various Rayleigh numbers at fixed parameters $\epsilon_s=0.1$, $D=0.5$, and $Pr=0.7$. (b) Effect of varying the compressibility parameters ϵ_s and Di at fixed $Ra=10^7$. As the parameters decrease toward the incompressible limit ($\epsilon_s, D\to 0$), the frequency of the acoustic oscillations increases. In all parameter regimes, the exponential decay confirms the absolute stability of the conduction state.

Evaluating the determinant for stationary modes ($\lambda=0$):

$$\det(\mathbf{M}) = -\frac{\gamma k^2}{\sqrt{PrRa}}\left[C_1(ik-\zeta)+\frac{1}{\epsilon_s}\right](\zeta m - ik). \tag{S15}$$

Because physical wavenumbers k must be strictly real, the determinant is never zero ($\det(\mathbf{M})\neq 0$) for any physical $k\neq 0$. This mathematical constraint fundamentally dictates that $\lambda=0$ is not a valid eigenvalue of the system, thereby precluding the existence of a stationary pitchfork bifurcation—the standard continuous transition (also called the principle of exchange of stabilities) required for the onset of classical Rayleigh-Bénard convection [7].

Instead, any instability in this 1D formulation must be strictly oscillatory. As the Rayleigh number increases, the system may undergo a Hopf bifurcation where the eigenvalues cross into the right half-plane with a non-zero imaginary component ($\mathrm{Im}(\lambda) \neq 0$). Physically, these growing oscillatory modes correspond to acoustic waves (sound waves) resonating between the vertical boundaries, a phenomenon known in stability theory as overstability. However, because the fluid is constrained to a single spatial dimension, these oscillations represent purely longitudinal expansions and compressions; fluid parcels merely oscillate in place and cannot physically go past each other. Consequently, macroscopic bodily overturning is geometrically impossible, preventing any sustained convective heat transport. Therefore, the critical Rayleigh number for the onset of steady, overturning convection is effectively infinite ($Ra_c \to \infty$).

B. Numerical Simulation Details

To numerically validate the theoretical stability of the conduction state derived above, we perform direct numerical simulations (DNS) of the fully compressible 1D governing equations. Because the 1D system supports high-frequency acoustic modes (overstability) and requires robust numerical dissipation to handle potential wave steepening without spurious oscillations, specialized numerical schemes are required.

For the spatial discretization of the convective fluxes, we employ the semi-discrete Kurganov-Tadmor (KT) scheme [8]. The KT scheme is a high-resolution, central-upwind method that effectively resolves steep gradients and acoustic waves without the computational overhead or complexity of Riemann solvers and characteristic decomposition. The diffusive terms (viscous and thermal conduction) are discretized using standard second-order central differences.

For temporal integration, the system is advanced using an explicit third-order Strong Stability Preserving Runge-Kutta (eSSPRK3) method [9]. This time-stepping scheme is specifically chosen to maintain the total variation-diminishing (TVD) properties of the KT spatial discretization, ensuring numerical stability even in the presence of strong acoustic oscillations.

The simulation is initialized with the analytically exact conduction state. To rigorously test the stability of this state and trigger the potential instability, a deterministic, large-amplitude macroscopic perturbation is applied strictly to the velocity field. Specifically, the initial velocity is prescribed as a single half-sine mode spanning the domain, $u(z, t = 0) = 0.1u_f \sin(\pi z/d)$, which introduces a massive initial kinetic energy injection of order $\mathcal{O}(0.1u_f)$ while inherently satisfying the no-slip boundary conditions at the walls. The temperature field is left unperturbed.

The temporal evolution of the flow is shown in figure S1. In figure S1(a), we fix the superadiabaticity $\epsilon_s = 0.1$, the dissipation number $D = 0.5$, and the Prandtl number $Pr = 0.7$, while varying the Rayleigh number from 10^4 to 10^7. Despite the severe initial excitation, the non-dimensionalized root-mean-square velocity exhibits an oscillatory, exponential decay for all Ra. To see the influence of compressibility, figure S1(b) presents the flow evolution for varying combinations of ϵ_s and Di at fixed $Ra = 10^7$. Notably, as the system approaches the incompressible approximation ($\epsilon_s, D \to 0$), the frequency of the acoustic oscillations significantly increases. However, the fundamental stabilizing behavior remains unchanged, while the macroscopic perturbation systematically dissipates. This unconditionally confirms the absolute stability of the conduction state against convective overturning at any Rayleigh number, effectively representing an infinite transient time to convection in 1D.

S2. THE DHARA SOLVER: INCOMPRESSIBLE IMPLEMENTATION FOR 2D, 3D, AND 4D

In contrast to compressible simulations in the 1D case, the higher-dimensional ($D \geq 2$) simulations reported in the paper are performed under the incompressible Oberbeck-Boussinesq approximation in Cartesian domains. To conduct these computationally demanding simulations, we utilized the Dhara solver, which is a general high-performance fluid solver initially developed for fully compressible turbulent convection [5, 10]. The present study employs the dedicated incompressible module. This section describes the numerical framework, algorithmic implementation, and the validation of the solver against standard benchmarks.

A. Governing equations and discretization

The solver integrates the incompressible Navier-Stokes equations coupled with the energy equation. For a D-dimensional Cartesian box, the non-dimensionalized equations are:

$$\nabla \cdot \boldsymbol{u} = 0, \tag{S16}$$

$$\frac{\partial \boldsymbol{u}}{\partial t} + (\boldsymbol{u} \cdot \nabla)\boldsymbol{u} = -\nabla p + \sqrt{\frac{Pr}{Ra}}\nabla^2 \boldsymbol{u} + T\hat{z}, \tag{S17}$$

$$\frac{\partial T}{\partial t} + (\boldsymbol{u} \cdot \nabla)T = \frac{1}{\sqrt{RaPr}}\nabla^2 T. \tag{S18}$$

The variables are non-dimensionalized using the domain height H, the free-fall velocity $u_f = \sqrt{\alpha g \Delta T H}$, and the free-fall time $t_f = H/u_f$.

Spatial discretization is performed on a staggered marker-and-cell (MAC) grid in the coordinates x, y, z in 3D, and w, x, y, z in 4D. This arrangement naturally prevents odd-even pressure decoupling. The grid is uniformly spaced in the periodic horizontal directions. However, to adequately resolve the steep gradients near the horizontal walls, it is stretched along the vertical (z) axis. The physical non-uniform vertical grid $z \in [0, H]$ is mapped from a uniform computational grid $\xi \in [0, 1]$ using the tangent-hyperbolic function

$$z = \frac{H}{2}\left[1 - \frac{\tanh[\chi(1 - 2\xi)]}{\tanh \chi}\right], \tag{S19}$$

where the stretching parameter is fixed at $\chi = 1.2$ for all DHARA simulations reported here. This mapping ensures fine resolution inside the boundary layers. Time integration is performed via a low-storage third-order Runge-Kutta (RK3) method, optimizing memory usage for large-scale simulations.

B. Numerical algorithm and parallelization

To enforce the incompressibility constraint, we utilize a fractional-step projection method. The pressure Poisson equation is solved in the spectral domain for all periodic directions. In our configuration, the horizontal directions are periodic, while the domain in the vertical direction (z) is bounded by solid walls. By applying a Fast Fourier Transform (FFT) in the periodic directions, the Poisson equation is reduced to a set of independent one-dimensional tri-diagonal systems along the z-axis. These systems are solved exactly and efficiently using the Tri-diagonal Matrix Algorithm (TDMA). This hybrid FFT-TDMA approach is ideally suited for rectangular geometries, providing spectral accuracy in the horizontal planes and robust handling of no-slip boundary conditions at the horizontal plates.

DHARA is implemented in Python, leveraging a modern high-performance software stack designed for heterogeneous computing environments. The array operations are written using `NumPy` for conventional CPU execution and `CuPy` for highly parallelized NVIDIA GPU acceleration. To achieve massive scale across supercomputing clusters, global domain decomposition is achieved using a slab decomposition strategy. Inter-node and inter-device communication is explicitly managed via the message passing interface using `mpi4py`. For large-scale data analysis, the solver utilizes the `h5py` library, dumping data in the HDF5 format. This architecture makes the solver entirely hardware-agnostic, allowing seamless scaling from single multi-GPU nodes to large-scale computing clusters with minimal configuration changes.

C. Code validation

To ensure the fidelity of the DHARA solver, we performed extensive benchmarking against established high-precision direct numerical simulation data from the literature for both 2D and 3D Rayleigh-Bénard convection in horizontally periodic domains.

For the 2D configuration, we compared our solver against the simulations of Zhu et al. [11] for $Pr = 1.0$. Table S1 presents the comparison of the Nusselt number for Rayleigh numbers ranging from $Ra = 10^8$ to 10^9. We note that for these specific Rayleigh numbers, an integration time of $t_{sim} = 1000$ free-fall times is sufficient to ensure that the kinetic energy is well converged. To verify numerical convergence and internal consistency, we computed the Nusselt number via four independent formulations: volume-averaged convective flux (Nu), wall-averaged temperature gradients (Nu_W), kinetic energy dissipation (Nu_{ε_u}), and thermal dissipation (Nu_{ε_T}). Their strong mutual agreement is detailed under the DHARA columns in table S1. We match the exact grid resolution ($N_x \times N_z$) and ensure a highly comparable number of grid points within the thermal boundary layer (N_{BL}) between both solvers. The results exhibit good quantitative agreement, demonstrating that our 2D spatial discretization accurately captures the flow dynamics. The large standard deviation of Nu around the mean value is a characteristic property of 2D convection [12].

		Zhu et al. [11]			Dhara					
Ra	Grid ($N_x \times N_z$)	t_{sim}	N_{BL}	Nu	t_{sim}	N_{BL}	Nu	Nu_W	Nu_{ε_u}	Nu_{ε_T}
10^8	512×256	1000	16	26.1	1000	15	24.7 ± 11.8	24.9 ± 1.1	23.4 ± 1.5	23.9 ± 1.8
2.15×10^8	768×384	1000	23	31.2	1000	23	31.0 ± 13.1	31.0 ± 1.2	30.7 ± 2.0	30.1 ± 1.8
4.64×10^8	768×384	1000	20	38.9	1000	21	38.0 ± 21.3	38.0 ± 1.8	37.8 ± 4.1	37.2 ± 2.5
10^9	1024×512	1000	25	48.3	1000	26	46.7 ± 27.1	46.8 ± 2.4	45.3 ± 7.3	46.1 ± 3.0

TABLE S1. Validation of the 2D solver against Zhu et al. [11] at $Pr = 1$ and an aspect ratio of $\Gamma = 2$.

For the 3D configuration, we benchmarked the solver against the highly resolved periodic-box data of Samuel et al. [13], who utilized a high-order spectral element method. We tested a domain with an aspect ratio of $\Gamma = 4$ for a fixed Prandtl number of $Pr = 0.7$. Table S2 compares the volume-averaged Nusselt number (Nu) and the root-mean-square Reynolds number (Re) for four decades of thermal driving ($Ra = 10^5$ to 10^8), along with the results of data for grid resolutions utilized. The macroscopic transport quantities computed by Dhara fall well within the statistical uncertainty of the reference spectral element data. This validation in both 2D and 3D provides confidence in the numerical accuracy and validity of the 4D extrapolations presented in the main text.

		Samuel et al. [13]			Dhara		
Ra	Grid	t_{sim}	Nu	Re	t_{sim}	Nu	Re
10^5	$128^2 \times 32$	1000	4.27 ± 0.24	93.0 ± 2.6	1000	4.31 ± 0.40	92.4 ± 3.1
10^6	$256^2 \times 64$	1000	8.15 ± 0.35	296 ± 5	1000	8.09 ± 0.61	298 ± 6
10^7	$512^2 \times 128$	1000	15.6 ± 0.9	892 ± 17	1000	15.8 ± 1.4	887 ± 18
10^8	$1024^2 \times 256$	1000	30.4 ± 1.9	2571 ± 47	1000	30.1 ± 2.6	2585 ± 52

TABLE S2. Validation of the 3D solver against the spectral element data of Samuel et al. [13] for a Cartesian box with horizontally periodic boundaries at $Pr = 0.7$ and an aspect ratio of $\Gamma = 4$.

S3. DEPENDENCE OF TRANSIENT TIME ON FLOW RESOLUTION AND GEOMETRY

As stated in the main text, high-Ra RBC simulations in closed domains are performed on coarser meshes than those required for faithfully studying various aspects of the flow. It is thus crucial to examine how the numerical resolution affects transient times.

In figure S2, we show the temporal evolutions of E in a closed cubic domain for $Pr = 1$ at Rayleigh numbers 10^8 and 10^9. Simulations are performed on grids with 120^3 and 200^3 mesh cells. E evolves similarly for all cases, with a rapid increase in the beginning, and overshooting its mean value before achieving a statistically steady state, in which it oscillates about E_{av}. This transient phase lasts for nearly 50 to 70 free-fall times. The mean kinetic energy in the steady state does not seem to depend strongly on the flow resolution. Therefore, conclusions drawn about the transient time on the basis of coarser simulations are not likely to change.

Figure S3 compares the evolutions of E for RBC in a unit cube with those in a rectangular cuboid of dimensions $L_x = 2.4H$ and $L_y = 0.8H$ [14]. Data for same Rayleigh numbers at $Pr = 1$ are shown. The figure illustrates that the evolutions of E are quite similar in the two domains, as in the resulting transient times.

[1] J. D. Anderson, *Computational Fluid Dynamics: The Basics with Applications* (McGraw-Hill, New York, 1995).
[2] J. Verhoeven, T. Wiesehöfer, and S. Stellmach, Anelastic versus fully compressible turbulent Rayleigh-Bénard convection, Astrophys. J. **805**, 97 (2015).
[3] J. P. John and J. Schumacher, Compressible turbulent convection in highly stratified adiabatic background, J. Fluid Mech. **972**, R4 (2023).

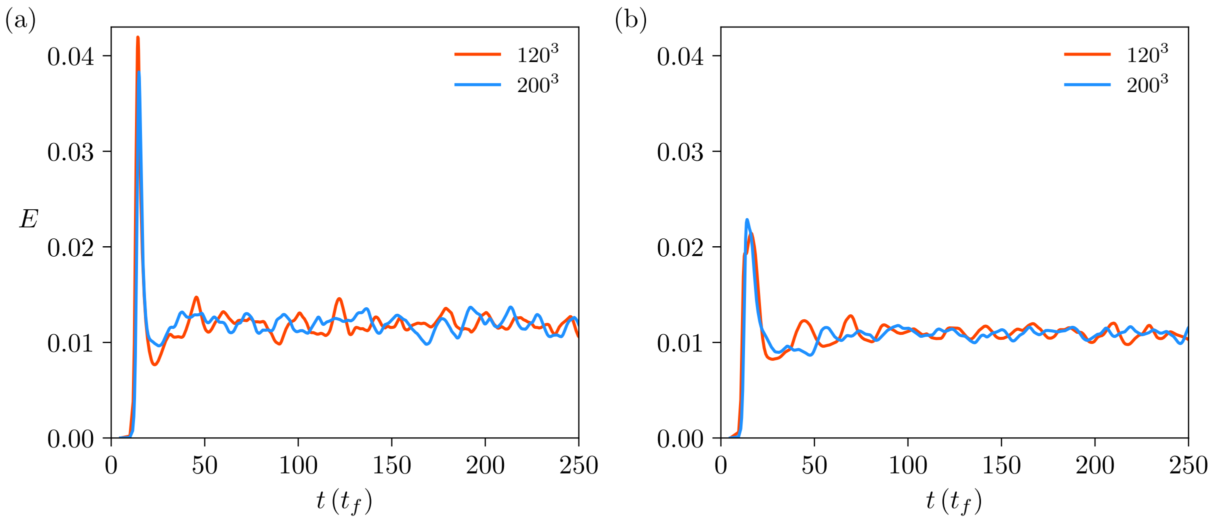

FIG. S2. Effects of grid resolution on evolution of E for RBC in a closed cube for $Pr = 1$: (a) $Ra = 10^8$ and (b) $Ra = 10^9$. The transient phase lasts for nearly 50 to 70 t_f and does not seem to strongly depend on the numerical resolution.

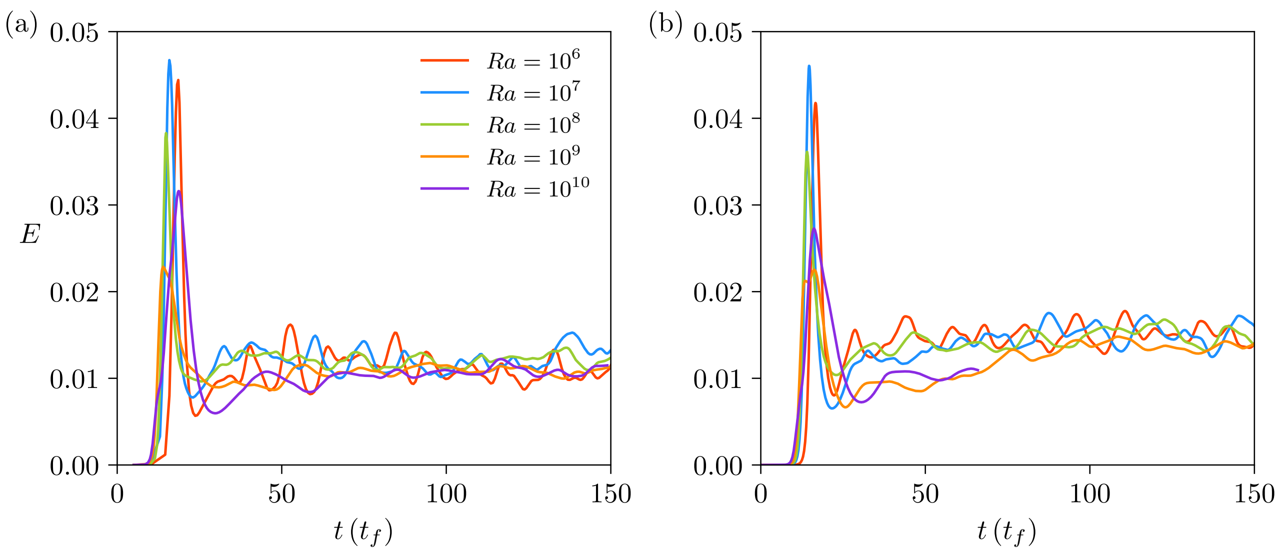

FIG. S3. Effects of domain shape on the evolution of E for $Pr = 1$. (a) RBC in a cubic box. (b) RBC in a rectangular cuboid [14]. The averaged kinetic energy evolves in a similar manner in the two domains, suggesting that the transient times do not depend strongly on the shape of the convection domain.

[4] J. P. John and J. Schumacher, Strongly superadiabatic and stratified limits of compressible convection, Phys. Rev. Fluids **8**, 103505 (2023).

[5] H. Tiwari, L. Sharma, and M. K. Verma, Compressible turbulent convection at very high Rayleigh numbers, Int. J. Heat Mass Transfer **242**, 126821 (2025).

[6] E. A. Spiegel and G. Veronis, On the Boussinesq approximation for a compressible fluid, Astrophys. J. **131**, 442 (1960).

[7] S. Chandrasekhar, *Hydrodynamic and Hydromagnetic Stability* (Oxford University Press, London, 1961).

[8] A. Kurganov and E. Tadmor, New high-resolution central schemes for nonlinear conservation laws and convection–diffusion equations, J. Comput. Phys. **160**, 241 (2000).

[9] S. Gottlieb, C.-W. Shu, and E. Tadmor, Strong stability-preserving high-order time discretization methods, SIAM Review **43**, 89 (2001).

[10] H. Tiwari, L. Sharma, and M. K. Verma, On the absence of the ultimate regime in turbulent thermal convection, Proc. Natl. Acad. Sci. U.S.A., **122** (44), e2513474122 (2025)

[11] X. Zhu, V. Mathai, R. J. A. M. Stevens, R. Verzicco, and D. Lohse, Transition to the ultimate regime in two-dimensional Rayleigh-Bénard convection, Phys. Rev. Lett. **120**, 144502 (2018).

[12] A. Pandey and K. R. Sreenivasan, Transient and steady convection in two dimensions, J. Fluid Mech. **1015**, A42 (2025).
[13] R. J. Samuel, M. Bode, J. D. Scheel, K. R. Sreenivasan, and J. Schumacher, No sustained mean velocity in the boundary region of plane thermal convection, J. Fluid Mech. **996**, A49 (2024).
[14] A. Pandey, J. Schumacher, M. Parsani, and K. R. Sreenivasan, Influence of plume activity on thermal convection in a rectangular cell, J. Fluid Mech. **1034**, A41 (2026).
[15] A. Pandey and M. K. Verma, Scaling of large-scale quantities in Rayleigh-Bénard convection, Phys. Fluids **28** (9), 095105 (2016).